Quasiparticle damping and the coherence peak in $YBa_2Cu_3O_{7-\delta}$

F. Gao,* G. L. Carr,† C. D. Porter, and D. B. Tanner
Department of Physics, University of Florida, Gainesville, Florida 32611

G. P. Williams and C. J. Hirschmugl‡
Brookhaven National Laboratory, Upton, New York 11973

B. Dutta, X. D. Wu,§ and S. Etemad
Bell Communications Research, Red Bank, New Jersey 07701
(Received 5 September 1995; revised manuscript received 15 January 1996)

The far-infrared (30–350 cm^{-1}) transmittance and reflectance of two *ab*-plane-oriented $YBa_2Cu_3O_{7-\delta}$ films have been measured. These data show that the quasiparticle relaxation rate, $1/\tau$, has a fast decrease below T_c and saturates at $T \ll T_c$. Above T_c, $1/\tau$ exhibits a linear temperature dependence, in accord with the linear dc resistivity in the normal state. The fast decrease of $1/\tau$ is unique and intrinsic to the high-T_c cuprates; it does not occur in conventional BCS superconductors, where the scattering is from impurity or phonons. The low-frequency conductivity σ_1 inferred from the far-infrared transmittance and reflectance measurements exhibits a peak just below T_c. The conductivity peak occurs at higher frequencies than those expected for BCS coherence effects. The peak in σ_1 is attributed to the rapid drop in $1/\tau$ combined with a decreasing normal-fluid density. [S0163-1829(96)04825-4]

I. INTRODUCTION

Temperature- and frequency-dependent measurements of the far-infrared conductivity $\sigma(\omega,T)$ played an important role in establishing the BCS mechanism of superconductivity.[1] The real part of the optical conductivity σ_1 is a measure of the rate at which particle-hole pairs are created by absorption of photons of frequency ω. For instance, the isotropic energy gap Δ in the excitation spectrum of an *s*-wave superconductor manifests itself as the absorption of photons at a threshold frequency $\omega=2\Delta$; there is no absorption below 2Δ for $T \ll T_c$. The gap was clearly seen, for example, in surface resistance[2] or optical conductivity[3] measurements of lead. As the temperature increases, the conductivity σ_1 at $\omega<2\Delta(T)$ is no longer zero, due to the existence of thermally excited quasiparticles. Moreover, the temperature dependence of the low-frequency conductivity exhibits a peak near T_c to coherence effects[4] that arises from the interference between the wave functions of the occupied states. Palmer and Tinkham[3] did indeed observe such an effect in $\sigma_1(\omega,T)$ for lead. A similar effect in the nuclear-spin-lattice relaxation rate in aluminum was observed by Hebel and Slichter.[5]

A difference between the optical conductivity and the spin-lattice relaxation is that the former depends on the relaxation rate of the carriers as well as coherence factors. In turn, the quasiparticle relaxation rate depends on the details of the mechanism that scatters the carriers. For instance, impurities and phonons are responsible for such scattering in ordinary metals. For many low-T_c superconductors, the transition temperature is much lower than the Debye temperature; thus, in dirty samples, impurity scattering is dominant, leading to a *T*-independent relaxation rate below T_c. When the purity is high, these materials enter the anomalous-skin-effect regime; here also the temperature dependence of the relaxation rate is not observed. Thus, in both the dirty and the anomalous-skin-effect regimes, the conductivity is dominated by the coherence factors, as is the spin-lattice relaxation.

In high-temperature superconductors, a similar-appearing ''coherencelike'' peak in σ_1 (or σ_1/σ_{1n}) has been observed. The peak has been seen in $YBa_2Cu_3O_{7-\delta}$ by Nuss *et al.*[6] at 0.5–2 THz using coherent time-domain terahertz spectroscopy, by Bonn *et al.*[7] at 2.95 GHz using cavity perturbation methods, and by Gao *et al.*[8] at 10 GHz using a parallel-plate-resonator technique. It has also been found in $Bi_2Sr_2Ca\ Cu_2O_8$ crystals by Holczer *et al.*[9] at 60 GHz using cavity methods and by Romero *et al.*[10] in infrared measurements.

Holczer *et al.*[9] attributed the peak to the consequence of ordinary case-II BCS coherence effects and concluded that the pairing was dominantly *s* wave. However, the absence of a Hebel-Slichter peak in NMR experiments[11–14] is evidence against the assignment of the conductivity peak to coherence effects, because the same coherence factors apply to the conductivity σ_1 and the nuclear relaxation rate $1/T_1$. (Indeed, Marsiglio[15] has pointed out that coherence effects can be suppressed within the framework of a strong-coupling theory, and it has been shown[16] that such a suppression of the coherence peak in $1/T_1$ also would occur in σ_1.)

Nuss *et al.*[6] suggested that the peak could be the result of competition between a growing lifetime and a declining density of states. However, the temperature dependence of the lifetime was not given. Romero *et al.*[10] extracted the quasiparticle relaxation rate $1/\tau$ in $Bi_2Sr_2CaCu_2O_8$ from the width of the residual conductivity $\sigma_1(\omega)$ in the superconducting state and found a dramatic decrease in $1/\tau$ below T_c. The peak in σ_1/σ_{1n} was assigned to the product of a decreasing quasiparticle density and an increasing $\tau(T)$. Bonn *et al.*[17] observed a pronounced and anomalous peak at ~38 K in the surface resistance R_s of $YBa_2Cu_3O_{7-\delta}$. The peak, which was also in the extracted $\sigma_1(T)$, was attributed to a collapse by

two orders of magnitude in $1/\tau$ below T_c. Gao *et al.*[8] deduced a decreasing scattering rate and a decreasing normal-fluid density below T_c from a two-fluid analysis of the microwave surface impedance data for $YBa_2Cu_3O_{7-\delta}$ films. The observed peak in σ_1/σ_{1n} was interpreted as a consequence of competition between these two factors. Such a fast drop in $1/\tau$ has also been found in $La_{2-x}Sr_xCuO_4$.[18] Other experiments, such as femtosecond optical transient absorption measurements using pulsed laser pump and probe techniques,[19–21] also showed a dramatic increase in the relaxation time τ below T_c for $YBa_2Cu_3O_{7-\delta}$, $Bi_2Sr_2Ca_2Cu_3O_{10}$, and $Nd_{2-x}Ce_xCuO_{4-y}$.

There are a few experiments where no anomaly in $1/\tau$ at T_c is reported. For instance, Collins *et al.*[22] obtained a constant $1/\tau$ by using a Gorter-Casimir formula for the quasiparticle density in their model for the infrared conductivity of $YBa_2Cu_3O_{7-\delta}$. By fitting infrared transmittance of $Bi_2Sr_2CaCu_2O_8$, Mandrus *et al.*[23] obtained a continuous T-linear $1/\tau$ down to temperatures well below T_c and found no sharp drop at T_c. Their conductivity did show a maximum at T_c for all frequencies below 70 cm^{-1}. The reason for the differences between these and the other experiments is not clear. It could be a difference in samples or it could be due to the assumptions used in the analysis of the measurements.

The effect of a rapid decrease in $1/\tau$ at T_c is apparently unique to high-T_c superconductors. It suggests that the dominant scattering in these systems is electronic in origin rather than from phonons or impurities. In this paper, to investigate the origin of the ''coherence peak'' in high-temperature superconductors, we examine and discuss the conductivities of two $YBa_2Cu_3O_{7-\delta}$ films determined by analysis of far-infrared transmittance and reflectance data. In agreement with earlier studies, a peak in $\sigma_1(T)$ just below T_c at low frequencies for both films is found. Moreover, in contrast to the T-linear dependence in the normal state, a sudden drop in $1/\tau(T)$ below T_c is observed from a two-fluid fit to the transmittance spectra. We believe these features are intrinsic to the CuO_2 planes of all cuprates. Our data show that the peak in σ_1 is due to the competition between a fast increasing τ and a decreasing normal-fluid density with decreasing temperature, rather than to coherence effects.

II. THEORY OF BCS COHERENCE PEAK

To aid in visualizing how a coherence peak occurs in σ_1 it is useful to review BCS theory. The condensed-state wave function is a linear combination of one-electron states with correlation among electrons of opposite momenta and spins. The perturbation Hamiltonian can be written as

$$H_1=\sum_{\mathbf{k}\mathbf{k}'} B_{\mathbf{k}'\mathbf{k}} c^{\dagger}_{\mathbf{k}'} c_{\mathbf{k}}. \tag{1}$$

Here the subscript $\mathbf{k}$ ($\mathbf{k}'$) represents the quantum state for momentum and spin, $c^{\dagger}_{\mathbf{k}'}$, and $c_{\mathbf{k}}$ are the quasiparticle creation and annihilation operators, and $B_{\mathbf{k}'\mathbf{k}}$ are matrix elements of the perturbation operator. In the normal state, each term in the sum is independent. When $T<T_c$, however, there exists phase coherence among the wave functions of the occupied one-electron states. This interference leads to $B_{\mathbf{k}'\mathbf{k}} = \pm B_{-\mathbf{k}'-\mathbf{k}}$, with the upper sign for ''case-I'' and the lower sign for ''case-II'' interactions, depending on whether the perturbation is *even* or *odd* under time reversal. The perturbation Hamiltonian for the interaction of electromagnetic radiation with matter is proportional to $\mathbf{p}\cdot\mathbf{A}$, where $\mathbf{p}$ is the momentum of the electrons and $\mathbf{A}$ is the vector potential of the external field. Because this term is *odd* with $\mathbf{p}$, it is a case-II interaction. (Other perturbations with *even* symmetry, such as ultrasonic attenuation, obey the case-I coherence factor.)

The optical conductivity is proportional to[1,4]

$$\sigma_1 \propto \int_{-\infty}^{\infty} F(\Delta,E,E')N_s(E)N_s(E+\hbar\omega) \times[f(E)-f(E+\hbar\omega)]dE. \tag{2}$$

Here, the function F is the coherence factor for scattering,[4]

$$F(\Delta,E,E')=\frac{1}{2}\left(1\mp\frac{\Delta^2}{EE'}\right), \tag{3}$$

Δ is the temperature-dependent energy gap, E is the quasiparticle energy measured from the Fermi level, $E'=E+\hbar\omega$, and $f(E)=[1+e^{E/kT}]^{-1}$ is the Fermi distribution function. The remaining term in Eq. (2) is $N_s(E)$, the superconducting density of states:

$$N_s(E)=N_n \mathrm{Re}\,\frac{|E|}{\sqrt{E^2-\Delta^2}}, \tag{4}$$

with N_n the one-spin density of states near E_F when the superconductor is in its normal state and Re standing for the real part. Equation (4) indicates that $N_s=0$ for $|E|<\Delta$. It diverges near Δ and approaches the normal-state value when $|E|\gg\Delta$. The optical conductivity, Eq. (2), is governed by both the density of states and the coherence factors.

The optical conductivity of a superconductor was calculated by Mattis and Bardeen.[24] This calculation is valid when the superconductor is either in the extreme anomalous ($\lambda\ll l$) or dirty limit ($l\ll\xi$), where l is the electron mean free path, λ is the magnetic penetration depth, and ξ is the coherence length. However, neither limit is satisfied in high-T_c cuprates. For instance, in $YBa_2Cu_3O_{7-\delta}$, typical values are $\lambda=1400$ Å, $l=100$ Å, and $\xi=15$ Å. Thus the high-T_c superconductors are in the normal-skin-effect, clean-limit regime. Leplae[25] has extended the Mattis-Bardeen theory into the clean- or intermediate-limit regime, putting σ_{1s} into a form that incorporates the normal-state conductivity σ_n, governed by the quasiparticle scattering rate $1/\tau$. Recently, Chang and Scalapino[26] gave a generalization of the Leplae equation. The optical conductivity calculated within this theory is shown in Figs. 1 and 2.

To compare with the $YBa_2Cu_3O_{7-\delta}$ data presented here, we have used the values $T_c=90$ K, $2\Delta(0)=3.5\ k_BT_c=220$ cm^{-1}, a BCS temperature dependence to $2\Delta(T)$, and an inelastic scattering rate $\hbar/\tau=2.8\ k_BT$. The latter behavior follows the temperature dependence of the normal state $1/\tau$. The interpretation of the result is direct. When $T\ll T_c$, there are almost no thermally excited quasiparticles and $\sigma_1(\omega)\sim 0$ up to $\omega=2\Delta$; above this frequency, $\sigma_1(\omega)$ begins to rise (see Fig. 1) due to dissociation of Cooper pairs by photon absorp-

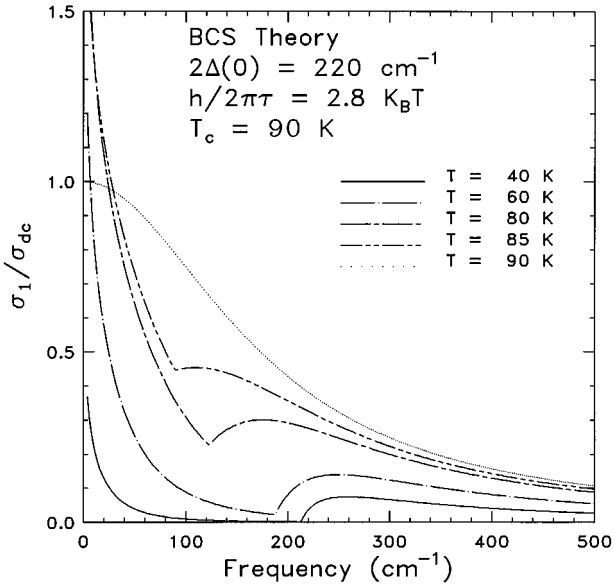

FIG. 1. The frequency-dependent conductivity of a superconductor in the framework of the BCS-Leplae formula. The curves are normalized by the dc conductivity of a normal metal having the same scattering rate.

tion, causing quasiparticle excitations from the superconducting condensate. $\sigma_{1s}(\omega)$ approaches $\sigma_{1n}(\omega)$ for $\omega \gtrsim 3\Delta(0)$ because the BCS density of states approaches the normal-state value, i.e., $N_s(E) \approx N_n(E)$ as expected in Eq. (4), at these excitation energies. Because of the gap, the oscillator strength at low frequencies is reduced; the ''missing'' area shifts to the origin to form the infinite dc conductivity of the superconducting condensate. As T increases, the minimum or threshold that signifies $2\Delta(T)$ moves to lower energies, due to a decrease of the superconducting gap. In addition, $\sigma_1(\omega) \neq 0$ for $\omega < 2\Delta(T)$ due to absorption by thermally excited quasiparticles. The low-frequency logarithmic upturn in Fig. 1 characterizes the case-II coherence effect.

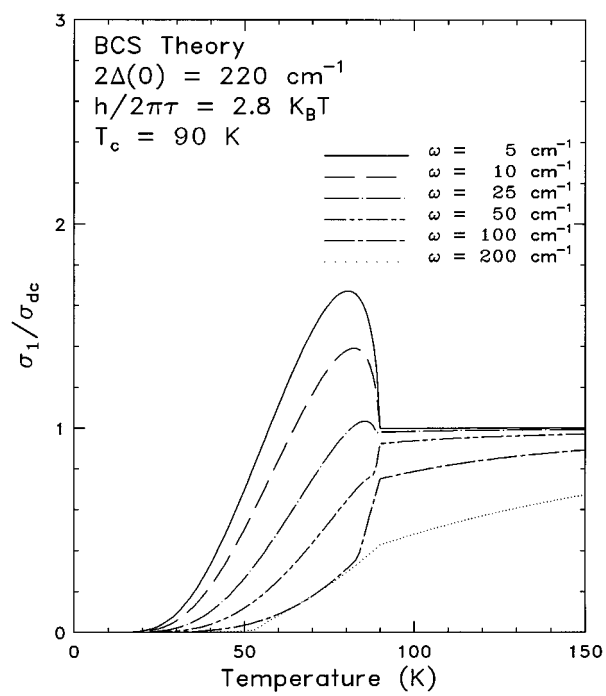

FIG. 2. The temperature dependence of the BCS conductivity at six selected frequencies. The curves are normalized by the dc conductivity of a normal metal having the same scattering rate. A coherence peak occurs just below T_c for $\omega \ll 2\Delta(0)$.

Figure 2 shows that, at small frequencies $\omega \ll 2\Delta$, the divergence of the BCS density of states $N_s(E)$ at $E \simeq \Delta$ in the integral of Eq. (2) causes a peak[27] in σ_1/σ_n below T_c. The conductivity eventually vanishes exponentially with decreasing temperature because the quasiparticles are frozen out. The magnitude of the peak falls monotonically with increasing frequency. The position of the peak shifts to slightly higher temperatures with increasing frequency. The peak gradually disappears as the photon energy is greater than the width of density-of-states peak. A discontinuity in the slope can be seen in Fig. 2 when T reaches a value such that $2\Delta(T) = \omega$. Above this temperature, the gap becomes smaller than the excitation frequency and an extra contribution to the integral comes from excitations across the gap. Experimental observations of coherence peaks in the nuclear relaxation rate[5] and optical conductivity[3] have strongly supported the BCS model for classical superconductors.

III. EXPERIMENT

The $YBa_2Cu_3O_{7-\delta}$ samples were c-axis oriented and grown epitaxially by pulsed-laser ablation[28] on 1-mm-thick single-crystal (100) MgO substrates of surface dimensions of 5×5 mm^2. The thicknesses of the films were 48 and 156 nm and the transition temperatures were 83 and 90 K, respectively. Details of the sample characteristics can be found elsewhere.[29]

The far-infrared (20–360 cm^{-1}) transmittance $\mathcal{T}(\omega)$ and reflectance $\mathcal{R}(\omega)$ measurements, over a range between 7 and 300 K were made using both the far-infrared beamline at the National Synchrotron Light Source[30] and a Bruker IFS-113v Fourier-transform interferometer with a Hg arc lamp source and a 4.2-K bolometer detector. The measurements were made at near-normal incidence, so that the far-infrared electric field is polarized along the *ab* plane. To deal with dispersive and absorptive effects in the substrate, the reflectance $\mathcal{R}_{\rm sub}$ and transmittance $\mathcal{T}_{\rm sub}$ of a bare MgO were carefully measured at each temperature where film data were taken. The absorption coefficient $\alpha(\omega)$ and the index of refraction $n(\omega)$ of the MgO were determined from $\mathcal{R}_{\rm sub}$ and $\mathcal{T}_{\rm sub}$ as described in the Appendix. These measurements were then used in analysis of the data for the films.

The optical response of a thin film, typically represented by $\mathcal{R}(\omega,T)$ and $\mathcal{T}(\omega,T)$, is governed by the electrical properties of the material such as the complex conductivity $\sigma = \sigma_1 + i(\omega/4\pi)(1-\epsilon_1) = \sigma_1 + i\sigma_2$. In other words, both $\mathcal{R}$ and $\mathcal{T}$ are functions of σ_1 and σ_2. Therefore, just a *single* optical measurement, $\mathcal{R}$ or $\mathcal{T}$, is not sufficient to determine both components of the conductivity unless one can measure that quantity in such a wide frequency range that the Kramers-Kronig transformation[31] can be performed, which is not always feasible especially for thin films on absorbing substrates. On the other hand, by measuring *both* the reflectance *and* transmittance of a film over any finite frequency range of interest, the conductivity $\sigma(\omega)$ can be extracted by

inverting $\mathcal{R}(\sigma_1,\sigma_2)$ and $\mathcal{T}(\sigma_1,\sigma_2)$. Unlike Kramers-Kronig analysis, in which the low-frequency conductivity is somewhat dependent on how the extrapolation of reflectance or transmittance to dc is made, in this approach the derived $\sigma(\omega)$ only depends on the accuracy of $\mathcal{R}(\omega)$ and $\mathcal{T}(\omega)$ at the same frequency point. The method of analyzing the data is described in detail in the Appendix.

IV. RESULTS AND DISCUSSION

A discussion of the transmittance and reflectance data has been given in a previous publication;[29] the reader is referred to that paper for details. In brief, the transmittance is very small ($\mathcal{T}<1\%$ for the thicker film) and somewhat influenced by the MgO substrate. Nevertheless, the signal-to-noise is good enough to allow our analysis without any data smoothing. Despite the complications of the substrate, one can clearly identify the intrinsic response of the $YBa_2Cu_3O_{7-\delta}$ films in the data. The transmittance approaches zero at low frequencies for $T<T_c$; from Eq. (A4) of the Appendix we infer that $|\sigma|\rightarrow\infty$ as $\omega\rightarrow 0$. The existence of a supercurrent in the film screens the applied electromagnetic field, so that there is no transmission at dc. There is finite transmittance at $\omega\rightarrow 0$ for $T>T_c$, corresponding to a finite optical conductivity. The low-frequency $\mathcal{R}(\omega)$ for both films approaches 100% in the superconducting state, but is well distinguished from unity at $T>T_c$. The experimental uncertainty in reflectance is about $\pm 1\%$, mainly on account of the difficulty in establishing precise optical alignment as the reference and the sample are interchanged.

A. Analysis of transmittance

1. Two-fluid behavior

Motivated by the higher accuracy in $\mathcal{T}(\omega)$ mentioned above, we began by fitting the transmittance data, extracting parameters in a dielectric function model for the system, including the quasiparticle scattering rate. To account for the non-Drude behavior of the optical conductivity, we used a two-component-model[32–38,29] for the complex dielectric function, $\epsilon(\omega)=1+4\pi i\sigma(\omega)/\omega$. In the normal state, $\epsilon(\omega)$ contains a narrow Drude band and a couple of broad mid-infrared Lorentzians,

$$\epsilon(\omega)=-\frac{\omega_p^2}{\omega^2+i\omega/\tau}+\sum_{j=1}^{2}\frac{\omega_{pj}^2}{\omega_j^2-\omega^2-i\omega\gamma_j}+\epsilon_\infty$$
$$=\epsilon_{\text{Drude}}+\epsilon_{\text{mid-ir}}+\epsilon_\infty \quad (T>T_c), \tag{5}$$

where ϵ_{Drude} describes the free-carrier response, with parameters ω_p the plasma frequency and $1/\tau$ the scattering rate, $\epsilon_{\text{mid-ir}}$ accounts for the absorption in the mid-infrared region, with parameters ω_{pj} the plasma frequency of the jth oscillator, which is at frequency ω_j and has width γ_j, and ϵ_∞ includes the contribution from excitations at frequencies above $\sim 1000\ \text{cm}^{-1}$.

In the superconducting state, a two-fluid analysis is used, assuming that a fraction (f_n) of the free carriers (the thermally excited quasiparticles) exhibit Drude behavior while the remaining part ($f_s=1-f_n$) condenses to form a δ function at $\omega=0$. The free carrier conductivity is generalized into

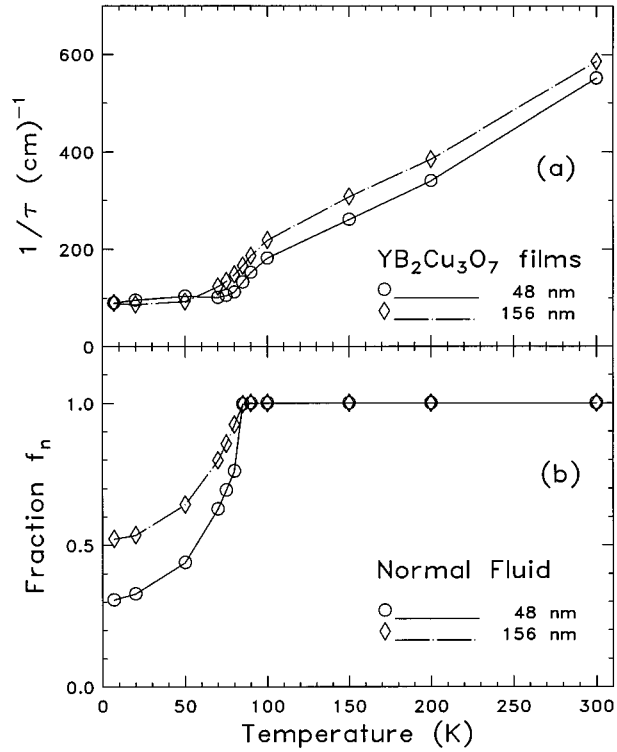

FIG. 3. The temperature dependence of two important Drude parameters obtained by fitting the transmittance data in a two-fluid analysis: (a) The relaxation rate, $1/\tau$. (b) The normal-fluid (or quasiparticle) density, $f_n(T)$.

$$\sigma=f_n\frac{\omega_p^2}{4\pi}\frac{\tau}{1-i\omega\tau}+f_s\frac{\omega_p^2}{4\pi}\left[\pi\delta(\omega)+i\frac{1}{\omega}\right]+\sigma_{\text{mid-ir}}, \tag{6}$$

with τ the quasiparticle relaxation time, and $\sigma_{\text{mid-ir}}$ the temperature-independent second-component (mid-infrared) contribution to the low-frequency conductivity. In this model the quasiparticles are the ''normal'' fluid; only these ''normal'' electrons contribute to σ_1 at finite frequencies. The ''super'' fluid gives an infinite σ_1 at dc ($\rho_{\text{dc}}=0$) as represented by the $\delta(\omega)$ function in Eq. (6) and has a purely inductive response at $\omega>0$. The details of the data fitting are described and the values of the fitting parameters given in Ref. 29. Here we are mainly interested in the temperature dependence of the quasiparticle density, $f_n(T)$, and the relaxation rate $1/\tau(T)$.

2. Relaxation rate and superfluid density

Figure 3 illustrates the two essential factors that govern the real part of the conductivity. The upper panel shows the relaxation rate $1/\tau$ for both $YBa_2Cu_3O_{7-\delta}$ films. When $T>T_c$, $1/\tau$ is nearly linear in temperature, with a nearly zero intercept. Such a T-linear behavior in $1/\tau$ above T_c has been observed previously by infrared measurements of $YBa_2Cu_3O_{7-\delta}$,[32,33] $Bi_2Sr_2CaCu_2O_8$,[10,32] and $La_{2-x}Sr_xCuO_4$.[18] This behavior in our samples shows once again that the well-known linearity in the dc resistivity $\rho(T)$ for the cuprate superconductors is caused by the temperature dependence of the relaxation rate; the carrier concentration is constant with temperature. Writing

$\hbar/\tau = 2\pi\lambda k_B T$, we can obtain a coupling constant $\lambda \approx 0.4$; taking $v_F = 2\times 10^7$ cm/sec, we can estimate the mean free path

$$l = v_F \tau \approx (60\ \text{Å})\ \frac{100\ \text{K}}{T}. \tag{7}$$

Because the *ab*-plane coherence length is less than 20 Å, Eq. (7) shows that the high-T_c oxides are clean-limit superconductors ($l > \xi$).

Below T_c, the scattering rate $1/\tau$ exhibits a sudden drop, with saturation at $T \lesssim 50$ K. This result suggests a strong suppression of the scattering channel at the superconducting transition. Presumably, the carrier-scattering process that is responsible for the T-linear resistivity in the normal state is suppressed when the free carriers condense. Other experiments that found a similar fast drop in $1/\tau$ include infrared measurements of $Bi_2Sr_2CaCu_2O_8$ (Ref. 10) and $La_{2-x}Sr_xCuO_4$,[18] microwave impedance measurements of $YBa_2Cu_3O_{7-\delta}$,[8,17] and time-resolved transient-absorption measurements of $YBa_2Cu_3O_{7-\delta}$ (Ref. 19) and $Nd_{2-x}Ce_xCuO_{4-y}$.[21] This striking feature seems to be a unique property of the copper-oxide superconductors, because ordinary phonon or impurity scattering, which dominate conventional superconductors, does not change dramatically at T_c. It is evidence that the quasiparticles interact with some spectrum of excitations which is affected by the onset of superconductivity, either the quasiparticle spectrum itself or another excitation that develops a gap at T_c.

The temperature dependence of the normal-fluid fraction $f_n(T)$ is shown in Fig. 3(b). It is these quasiparticles that account for the finite absorption, e.g., the nonzero $\sigma_1(\omega,T)$, at low frequencies. The superconducting fraction $f_s = 1 - f_n$ represents the condensed carriers that screen the electromagnetic field.

There are several possible interpretations of the remnant f_n when $T \to 0$. First, it could be caused by a defect region in the film that remains normal at low temperatures, perhaps at the $YBa_2Cu_3O_{7-\delta}$/MgO interface or perhaps at the twin boundaries. Second, it could be attributed to the chains. There is increasing evidence that in high-quality samples the chain states are metallic and even superconducting but that in twinned and oxygen-deficient samples they contribute to finite-frequency absorption.[39] Third, there could be incomplete condensation. There is a definite tendency for the superfluid density to be slightly smaller than the normal-state free-carrier density in both $YBa_2Cu_3O_{7-\delta}$ (Ref. 32) and other cuprates.[10,18] Fourth, the remnant f_n could be associated with nodes in the superconducting gap, such as might occur in a d-wave superconductor.[40,41] If the gap has nodes, then some quasiparticles have zero excitation energy and the superconducting gap absorption would begin at zero frequency. We note that microwave measurements[17] have frequently found a finite $\sigma_1(\omega)$, consistent with any of these ideas.

In turn, the cause of the remnant f_n at low temperatures affects the interpretation of the low-temperature values of $1/\tau$. If $1/\tau$ represents the quasiparticle scattering rate, then our films are in the clean limit at low temperatures, but not in the extreme clean limit. (The $\sim 90\ \text{cm}^{-1}$ scattering rate at low temperatures falls between the 40 and 60 K values used in Fig. 1.) Therefore, a gap feature would be observable, if it were present. In contrast, if the low-temperature values of $1/\tau$ is attributed to defect states, such as heavily twinned chains or a region in the film that remains normal at low temperatures, then the quasiparticle damping rate (which governs the superconducting-state conductivity) could be substantially less and the clean-limit argument would hold. Finally, if the gap has nodes, then the finite low-frequency conductivity and damping reflects the response of the quasiparticle states with small excitation energies.

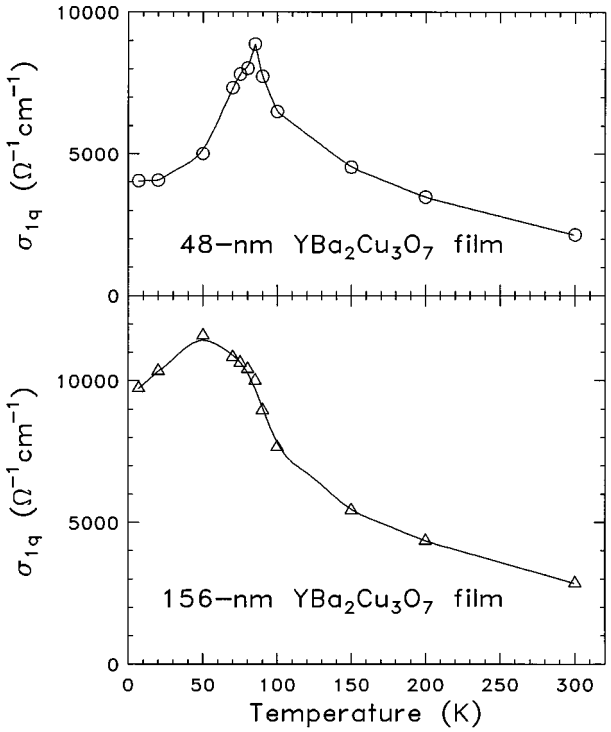

FIG. 4. The quasiparticle conductivity from model fit to the transmittance as described in the text.

The zero-temperature value of $1/\tau$ is larger than the extrapolated intercept of the linear regime above T_c (90 cm^{-1} vs 20 cm^{-1}). For this reason we tend towards the extrinsic explanation of the remnant f_n and low-temperature values of $1/\tau$.

3. Conductivity peak

From the quasiparticle density and the relaxation rate, we can calculate the low-frequency ($\omega \ll 1/\tau$) conductivity, which we call the quasiparticle conductivity, σ_{1q}. We use a simple model, a Drude formula at $\omega = 0$:

$$\sigma_{1q} = f_n \omega_p^2 \tau / 4\pi. \tag{8}$$

The results for both films are shown in Fig. 4. σ_{1q} is enhanced above the normal-state value and a peak is seen below T_c. It is the fast drop in $1/\tau$ that causes the peak in σ_{1q}. That it is due to changes in τ and not to BCS coherence effects is consistent with the absence of a coherence peak in the nuclear relaxation rate.[12] The peak occurs because of the competition between a decreased number of quasiparticles and an increased relaxation time (τ) with decreasing temperature. In contrast, the NMR relaxation rate $1/T_1$ does not depend on τ.

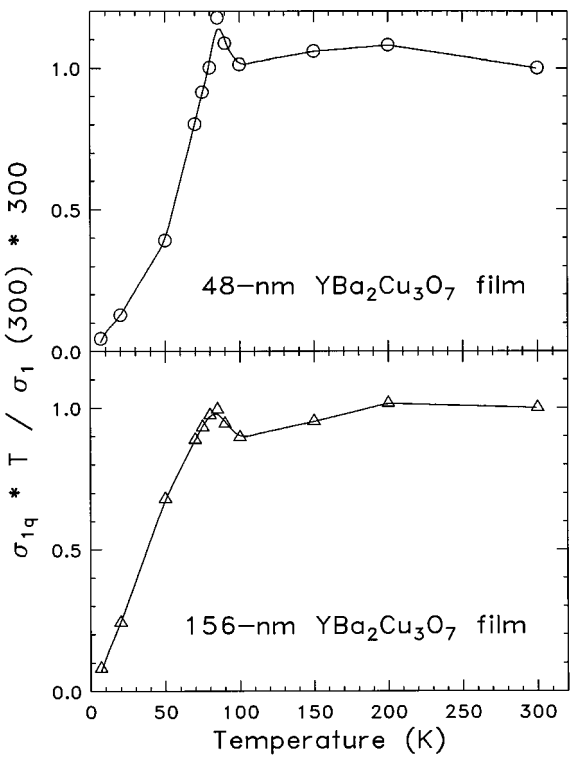

FIG. 5. The quasiparticle conductivity multiplied by the temperature, The results are obtained from model fit to the transmittance as described in the text. The quantities are normalized to their 300 K values.

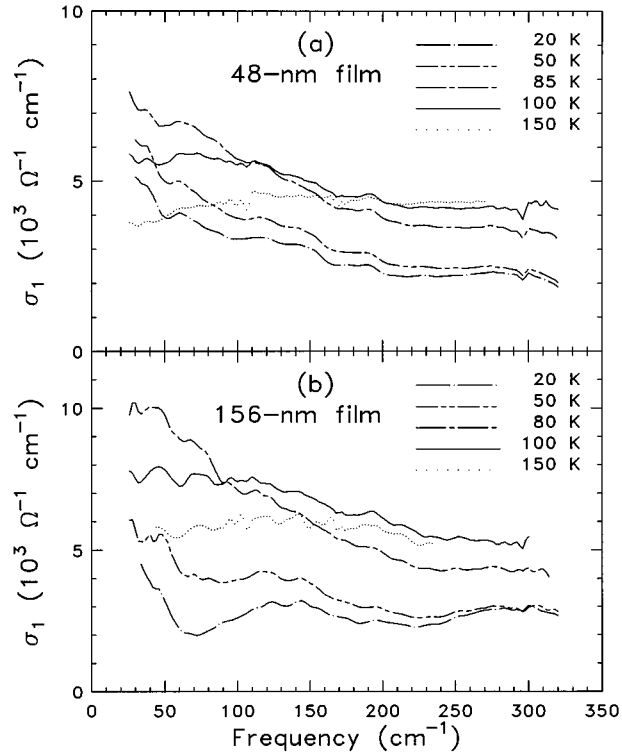

FIG. 6. The real part of the optical conductivity extracted directly from the experimental transmittance and reflectance of the 48-nm (a) and 156-nm (b) $YBa_2Cu_3O_{7-\delta}$ films.

The peak in σ_{1q} is more clearly seen if the broad $1/T$ dependence of the normal state $\sigma_1(\omega)$ is removed. We remove this dependence by plotting $T\sigma_{1q}$, as shown in Fig. 5. The curves are normalized to their 300 K values. For each sample, there is a rather sharp maximum just below T_c.

B. Conductivity from transmittance and reflectance

1. Discussion of uncertainties

In this section we turn to an analysis of the conductivity as obtained from the reflectance and transmittance data. Note that the absolute $\sigma_1(\omega)$ obtained from $\mathcal{R}$ and $\mathcal{T}$ has large error bars when the reflectance is close to unity. These errors occur because, according to the Appendix,

$$\sigma_1 \propto \frac{1-\mathcal{R}_f-\mathcal{T}_f}{\mathcal{T}_f}, \tag{9}$$

with $\mathcal{R}_f$ and $\mathcal{T}_f$ being, respectively, the reflection from and transmission through the film on the substrate. At low temperatures, $\mathcal{R}_f \approx 1$ and $\mathcal{T}_f \ll 1$. Under these conditions, the uncertainty in the conductivity due to systematic errors in the reflectance level is $\Delta\sigma_1/\sigma_1 \approx -\Delta\mathcal{R}_f/(1-\mathcal{R}_f)$. Thus, the accuracy of σ_1 suffers significantly when $\Delta\mathcal{R}_f \sim 1-\mathcal{R}_f$, as is true at low temperatures and low frequencies. A similar problem occurs in the Kramers-Kronig analysis of highly reflecting samples.[18,32,33] In contrast, the relative errors in the transmittance are much smaller than the errors in $1-\mathcal{R}$, so that the contributions to the errors in $\sigma_1(\omega)$ from $\mathcal{T}(\omega)$ are generally much smaller than those from $\mathcal{R}(\omega)$.

Because the errors in $\mathcal{T}(\omega)$ are smaller, we have adopted the following strategy to scale the reflectance data. We use the parameters of the fit to the transmittance data, discussed above, to calculate the reflectance of our samples. We then scale the measured reflectance so that there is a match at low ω between the calculated and the measured values. The difference between the experimental and calculated $\mathcal{R}(\omega)$ is less than 1%, i.e., less than the estimated uncertainty of the measured reflectance. This scaling has a significant impact on the results of $\sigma_1(\omega)$ in the superconducting state, when $\mathcal{R}(\omega) \approx 1$ whereas the influence is negligible in the normal state, when $\mathcal{R}(\omega)$ is well below unity. After scaling the reflectance, we proceed to extract the optical conductivity from the reflectance and transmittance, following the scheme outlined in the Appendix.

2. Conductivity spectrum

The real part of the conductivity $\sigma_1(\omega)$ is depicted in Fig. 6. In the normal state, $\sigma_1(\omega)$ approaches the ordinary dc conductivity at low frequencies. It deviates, however, from a Drude response at higher frequencies because of the well-known mid-infrared absorption.[34] In the superconducting state, the Drude component condenses; the spectral weight loss can be seen for $T<80$ K, implying a shift of weight to the origin. The remaining conductivity at $T \ll T_c$ can be partly attributed to the low-frequency tail of the broad mid-infrared component and partly to a remnant Drude absorption. Focusing on the data below 100 cm^{-1}, which characterize primarily the free-carrier response, we note that σ_1 initially increases with decreasing temperature, reaching a maximum at around 80 K, and then falls again at lower temperature.

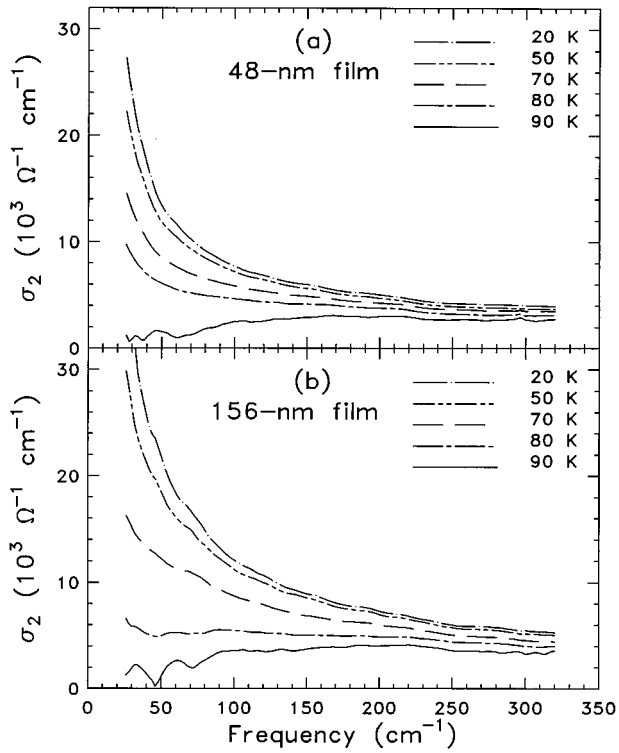

FIG. 7. The imaginary part of the conductivity at temperatures near T_c and below.

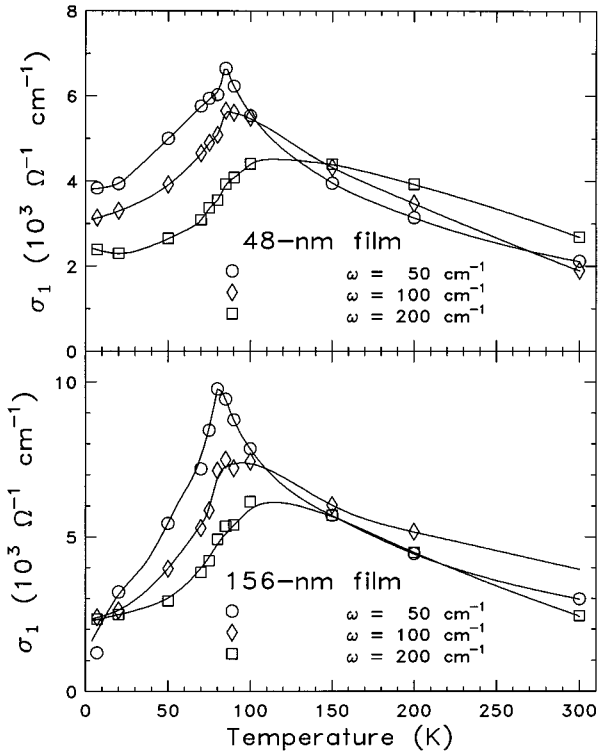

FIG. 8. The temperature dependence of the conductivity at three selected frequencies for two $YBa_2Cu_3O_{7-\delta}$ films.

The imaginary part σ_2 near and below T_c is plotted in Fig. 7. It decreases monotonically with increasing temperatures, indicating a loss of superfluid carriers. At low frequencies $\sigma_2 > \sigma_1$, indicating that the inductive current dominates over the conduction current in the superconducting state. For $T=90$ K ($\sim T_c$), $\sigma_2(\omega)$ extrapolates to the origin, as expected for a normal metal. A change of slope at the superconducting transition can be seen in the figure.

When $T \ll T_c$, σ_2 follows an A/ω dependence for $\omega \leqslant 100$ cm^{-1}, where A is a constant. This behavior is consistent with a local electrodynamic description of $\sigma_2 = c^2/4\pi\lambda_L^2\omega$, where λ_L is the London penetration depth. From these data, we obtain $\lambda_L \approx 2200 \pm 200$ Å for our films. This value is a little larger than the 1800 Å estimated[32] from Kramers-Kronig analysis of thicker films on $SrTiO_3$, which again suggests incomplete condensation in our films. When $\omega \geqslant 120$ cm^{-1}, σ_2 falls off more slowly than $1/\omega$, on account of both the broad mid-infrared contribution and a remaining normal Drude component.

3. Conductivity peak

The temperature-dependent $\sigma_1(T)$ at low frequencies exhibits a peak below T_c. This peak was already seen in Fig. 6 and can be better illustrated in the plot of σ_1 as a function of temperature shown in Fig. 8. The peak decreases in height with increasing frequency and gradually disappears at $\omega > 100$ cm^{-1}. This peak resembles both the one in σ_{1q} shown in Fig. 4 and the feature in conventional superconductors arising from the case-II coherence factors, shown in Fig. 2. We have already argued that it should *not* be attributed to a coherence effect, based on the absence of a peak in the NMR data. The peak in the high-T_c materials also differs from the BCS calculation in two ways. First, the BCS coherence peak occurs only at very low frequencies $[\omega/2\Delta(0) \lesssim 0.1]$ (see Fig. 2), whereas the peak in $YBa_2Cu_3O_{7-\delta}$ occurs clearly at 50 cm^{-1}, which would be almost a quarter of $2\Delta(0)$ if the BCS gap value is used. Second, the BCS conductivity peak occurs very near T_c and changes only slightly with frequency. For instance, the peak occurs at 0.8 T_c at very low frequencies (1 GHz), at 0.88 T_c for $\omega=5$ cm^{-1} (170 GHz), and at higher temperatures still for higher frequencies. In contrast, Bonn *et al.*[17] have found a microwave conductivity peak occurs at 0.4 T_c in $YBa_2Cu_3O_{7-\delta}$ crystals; we find a peak at ≈ 0.9 T_c at 50 cm^{-1}. Therefore, the peaks observed in the high-T_c cuprates are fundamentally different from that of the BCS coherence peak.

The peak in σ_1 has implications for the mechanism of quasiparticle scattering. The decrease in $1/\tau$ seen in Fig. 3 suggests that the excitations responsible for the scattering of the free carriers are suppressed when the free carriers condense. Evidently, the charge carriers interact with some spectrum of excitations which is affected by the onset of superconductivity. One possible explanation would attribute the scattering to the free carriers themselves, making the scattering be some kind of electron-electron scattering. This scattering would then follow

$$1/\tau = f_n(T) n \boldsymbol{\sigma}_{\mathbf{ee}} v_F, \tag{10}$$

where n is the carrier density, v_F the Fermi velocity, f_n the fraction of thermally excited quasiparticles, and $\boldsymbol{\sigma}_{\mathbf{ee}}$ the cross section for electron-electron scattering. Equation (10) essentially states that the scattering rate is given by a product of a cross section for scattering with the number of scattering

centers. In the normal state, $f_n=1$ and so the cross section $\boldsymbol{\sigma}_{\mathbf{ee}}$ varies linearly with T above T_c and (presumably) also varies linearly with T below T_c. The rapid drop in $1/\tau$ just below T_c would then be due to the decrease in f_n as the free carriers condense.

Although it may be plausible, this picture does not lead to a peak in conductivity, because the low-frequency conductivity is

$$\sigma_1=f_n\frac{ne^2\tau}{m^*}=\frac{e^2}{m^*v_F\boldsymbol{\sigma}_{\mathbf{ee}}}, \tag{11}$$

where e is the electronic charge and m^* the effective mass. According to Eq. (11), electron-electron scattering gives *no* peak in σ_1. Instead, the drop in $1/\tau$ is canceled by the drop in f_n. That the peak exists implies that $1/\tau$ falls more rapidly than f_n near T_c. We speculate that either (1) coherence effects do influence the quasiparticle conductivity near T_c (but differently than BCS-type s-wave coherence factors since coherence effects are not seen in NMR data[11–14]) or (2) the scattering is not from the free carriers but instead from another excitation which develops a gap at T_c. In an RVB scenario,[42] for example, one could attribute the scattering of the holons (the charge carriers) to spinon excitations, and expect a different temperature dependence for holon and spinon densities below T_c. Our measurements cannot decide between these two possibilities, but do suggest that one or the other is the case.

V. CONCLUSIONS

In summary, we have examined the far-infrared conductivity $\sigma(\omega)$ below 350 cm^{-1} obtained from transmittance and reflectance measurements of $YBa_2Cu_3O_{7-\delta}$ thin films. We have shown—in both direct analysis of $\mathcal{T}(\omega)$ and $\mathcal{R}(\omega)$ and in calculations using parameters obtained from a fit to the transmittance—that the real part of the conductivity, σ_1, exhibits a peak just below T_c. Based on the behavior of the quasiparticle density and relaxation rate and on comparison with BCS calculations, we conclude that the enhancement in σ_1 below T_c for the high-T_c cuprates differs from the BCS ''coherence peak.'' In the BCS superconductor, there is an enhanced optical conductivity due to scattering of quasiparticles into the large density of states near an energy of Δ above the Fermi energy. We believe that in the cuprates the sudden drop in $1/\tau$ upon superconducting transition combines with the decreasing number of quasiparticles to govern the conductivity peak. This interpretation is consistent with the absence of a coherence peak in the NMR relaxation rate $1/T_1$ for $YBa_2Cu_3O_{7-\delta}$.

The collapse of carrier scattering at T_c is fundamentally different from the behavior of phonon or impurity scattering. It implies a suppression of the scattering channel or the development of a gap in the spectrum of excitation that is responsible for the normal-state transport. It also suggests that an electronic interaction between the charge carriers is dominant in the superconducting state.

ACKNOWLEDGMENTS

The work at Florida is supported by National Science Foundation, Condensed Matter Physics Program, Grant No. DMR-9403894.

APPENDIX

This appendix illustrates how we can find an analytic solution for the complex conductivity $\sigma(\omega)$ from measurements of the transmittance and reflectance of a thin film on a thick substrate and of a blank substrate.

1. Boundary-value problem for a thin film on a thick substrate

For the case of a film of thickness $d\ll\delta<\lambda$, where δ is the skin or penetration depth and λ is the wavelength of the far-infrared radiation, the film may be idealized as a surface sheet of current $\mathbf{K}=\mathbf{J}d=\sigma\mathbf{E}d$. In this case, the current density $\mathbf{K}$ or $\mathbf{J}$ and the $\mathbf{E}$ and $\mathbf{H}$ fields are essentially constant throughout the thickness of the film. The boundary conditions require that the tangential components of $\mathbf{E}$ be continuous across the film, and that the tangential components of $\mathbf{H}$ be discontinuous by the surface current in the film. For normal incidence, the following relations are therefore satisfied:

$$\begin{aligned}1+r_f-t_f&=0,\\ 1-r_f-nt_f&=(4\pi/c)\sigma dt_f,\end{aligned} \tag{A1}$$

where t_f is the amplitude coefficient of transmission across the film into a nonabsorbing substrate with index n, and r_f is the single-bounce amplitude coefficient of reflection from the film.

By solving Eq. (A1), one obtains

$$\begin{aligned}t_f&=\frac{2}{1+(y+n)},\\ r_f&=\frac{1-(y+n)}{1+(y+n)}.\end{aligned} \tag{A2}$$

Here we have introduced a dimensionless complex admittance for the thin film, $y=Z_0\sigma d$ or $y_1+iy_2=Z_0(\sigma_1+i\sigma_2)d$, where $Z_0=377\ \Omega=4\pi/c$ (esu) is the impedance of free space. From $\mathcal{T}_f=n|t_f|^2$ and $\mathcal{R}_f=|r_f|^2$ we can calculate the power transmission and reflection coefficients:[43]

$$\begin{aligned}\mathcal{T}_f&=n|t_f|^2=\frac{4n}{(y_1+n+1)^2+y_2^2},\\ \mathcal{R}_f&=|r_f|^2=\frac{(y_1+n-1)^2+y_2^2}{(y_1+n+1)^2+y_2^2}.\end{aligned} \tag{A3}$$

Note that when $y_1\gg n+1$ or $\mathcal{T}_f\ll\mathcal{T}_s=4n/(n+1)^2$, the transmittance when $y=0$, then

$$\mathcal{T}_f\approx\frac{4n}{|y|^2}, \tag{A4}$$

so that the transmittance is a measure of the sheet impedance $Z=1/\sigma d$ of the film.

2. Exact expressions for t_f and r_f

The optical constants can also be extracted from general expressions for the complex Fresnel coefficients for the normal incidence transmission and reflection. A thin film on a substrate is a three-medium system, the air, the film, and the

substrate, with complex refractive indices of N_1, N_2, and N_3, respectively, where $N_j = n_j + i\kappa_j$ $(j=1,2,3)$. The amplitude transmission coefficient (from medium 1 through medium 2 and into medium 3) is

$$t_f = \frac{t_{12}t_{23}e^{i\phi}}{1 - r_{23}r_{21}e^{i2\phi}}, \tag{A5}$$

where $r_{ij} = (N_i - N_j)/(N_i + N_j)$ and $t_{ij} = 2N_i/(N_i + N_j)$ are the amplitude coefficients of reflection and transmission for a *single interface*. Note $r_{ji} = -r_{ij}$ and $1 + r_{ij} = t_{ij}$. The remaining quantity in Eq. (A5), the complex phase depth ϕ of medium 2 (the film) with thickness d, is given by $\phi = N_2\omega d/c$. Similarly, the amplitude reflection coefficient is

$$r_f = \frac{r_{12} + r_{23}e^{i2\phi}}{1 - r_{23}r_{21}e^{i2\phi}}. \tag{A6}$$

Note the identity $t_{12}t_{21} - r_{12}r_{21} \equiv 1$ has been used in deriving Eq. (A6). The denominators in Eqs. (A5) and (A6) account for the multiple internal reflections in the film. The power transmittance and reflectance is then $\mathcal{T}_f = (n_3/n_1)|t_f|^2$ and $\mathcal{R}_f = |r_f|^2$.

On substitution of the expression for r_{ij} and t_{ij} into Eqs. (A5) and (A6), one finds

$$t_f = \frac{4N_1N_2}{(N_1+N_2)(N_2+N_3)e^{-i\phi} - (N_2-N_3)(N_2-N_1)e^{i\phi}} \tag{A7}$$

and

$$r_f = \frac{(N_1-N_2)(N_2+N_3)e^{-i\phi} + (N_2-N_3)(N_1+N_2)e^{i\phi}}{(N_1+N_2)(N_2+N_3)e^{-i\phi} - (N_2-N_3)(N_2-N_1)e^{i\phi}}. \tag{A8}$$

One can reduce the rigorous expressions of Eqs. (A5)–(A8) to an approximation of the form of Eq. (A3) by taking medium 1 as vacuum ($N_1 = 1$), medium 2 as a metal film with a thickness d and a refractive index N_2, and medium 3 as a weakly absorbing semi-infinite slab with an index N_3. Then, in the long-wavelength (or low-frequency) limit when the film is thin enough that $\phi \ll 1$,

$$\begin{gathered} |N_2| \gg N_1 = 1, \\ |N_2| \gg |N_3| \approx n_3 \equiv n, \quad (\kappa_3 \ll n_3) \\ e^{\pm i\phi} \approx 1 \pm i\phi, \\ -iN_2\phi = -i\,\frac{\omega}{c}\,\epsilon d \approx \frac{4\pi}{c}\,\sigma d = y. \end{gathered} \tag{A9}$$

Using the relations in Eq. (A9), the denominator $\mathcal{D}$ in Eqs. (A7) and (A8) can be simplified to

$$\mathcal{D} \approx 2N_2(1 + n + y) \tag{A10}$$

and the numerator $\mathcal{N}$ in Eq. (A8) to

$$\mathcal{N} \approx 2N_2(N_1 - N_3 - y) = 2N_2(1 - n - y). \tag{A11}$$

Finally, one arrives at

$$t_f \approx \frac{2}{1 + n + y} \tag{A12}$$

and

$$r_f \approx \frac{1 - n - y}{1 + n + y}. \tag{A13}$$

The results of Eq. (A2) are recovered. These equations may also be viewed as generalizations of the single interface expressions, taking $(y + n)$ as a total effective surface admittance for the *parallel* film-substrate composite.

The accuracy of the above approximation has been tested by calculating t_f and r_f from the obtained n (or N_3) and y (or N_2) using the *approximate* form Eq. (A2) and the *exact* Eqs. (A5) and (A6). In the worst case, the results differ by less than 1% throughout the frequency regime up to 300 cm^{-1}.

3. The effect of the substrate

In reality, the substrate has a finite thickness and thus ours is a four-medium problem, with medium 4 being air. In the following, we assume a thick or wedged substrate, so that there is no phase coherence among multiple internal reflections within the substrate. This assumption means that we only need to add the power intensities, rather than the amplitudes. The directly measurable quantities of this four-medium system are the total transmittance and reflectance,

$$\begin{gathered} \mathcal{T} = \frac{(1 - \mathcal{R}_s)e^{-\alpha x}}{1 - \mathcal{R}_s\mathcal{R}_f' e^{-2\alpha x}}\,\mathcal{T}_f, \\ \mathcal{R} = \mathcal{R}_f + \frac{(1 - \mathcal{R}_s)^2\mathcal{R}_s e^{-\alpha x}}{1 - \mathcal{R}_s\mathcal{R}_f' e^{-2\alpha x}}\,\mathcal{T}_f, \end{gathered} \tag{A14}$$

where x is the thickness and α the absorption coefficient of the substrate. The other terms in Eq. (A14) are the substrate-incident internal reflection of the film,

$$\mathcal{R}_f' = \frac{(y_1 - n + 1)^2 + y_2^2}{(y_1 + n + 1)^2 + y_2^2}, \tag{A15}$$

and the single-bounce reflection of the substrate,

$$\mathcal{R}_s = \frac{(1-n)^2 + \kappa^2}{(1+n)^2 + \kappa^2} \approx \left(\frac{1-n}{1+n}\right)^2. \tag{A16}$$

The approximation in Eq. (A16) holds when $\kappa \equiv c\alpha/2\omega \ll n$, the case for weakly absorbing media.

4. Analytical solutions

We next want to find the explicit analytical solution for $y = y_1 + iy_2$ (and thus for σ_1 and σ_2) from Eqs. (A3) and (A14). According to Eq. (A3), the real part y_1 can be easily extracted from $\mathcal{T}_f$ and $\mathcal{R}_f$ as

$$y_1 = n\,\frac{1 - \mathcal{R}_f - \mathcal{T}_f}{\mathcal{T}_f}. \tag{A17}$$

However, the directly measured quantities are not $\mathcal{T}_f$ or $\mathcal{R}_f$, but $\mathcal{T}$ and $\mathcal{R}$, the total transmittance and reflectance. In

practice, we usually have $\mathcal{R}_f \approx \mathcal{R}$. But we can use the exact form in terms of $\mathcal{T}$ and $\mathcal{R}$ as well as the extracted substrate parameters:

$$\mathcal{R}_f = \mathcal{R} - \mathcal{T}(1-\mathcal{R}_s)\mathcal{R}_s e^{-\alpha x} = \mathcal{R} - \Delta\mathcal{R}. \tag{A18}$$

The expression for $\mathcal{T}_f$ is more complicated because it involves a new unknown quantity $\mathcal{R}_f'$ that we now try to find.

We first solve for $\mathcal{R}_f'$ in terms of $\mathcal{T}_f$ and $\mathcal{R}_f$ and n using Eqs. (A3), (A15), and (A17), which gives

$$\mathcal{R}_f' = 1 - \frac{4n(y_1+1)}{(y_1+n+1)^2+y_2^2} = 1-(y_1+1)\mathcal{T}_f$$
$$= 1 - n(1-\mathcal{R}_f) + (n-1)\mathcal{T}_f. \tag{A19}$$

On substitution of $\mathcal{R}_f'$ into the expression for $\mathcal{T}$ in Eq. (A14), a *linear* equation for $\mathcal{T}_f$ in terms of $\mathcal{T}$ and $\mathcal{R}$ and substrate parameters can be deduced:

$$\mathcal{T}\{1-\mathcal{R}_s[1-n(1-\mathcal{R}_f)+(n-1)\mathcal{T}_f]e^{-2\alpha x}\}$$
$$= (1-\mathcal{R}_s)e^{-\alpha x}\mathcal{T}_f. \tag{A20}$$

The solution is

$$\mathcal{T}_f = \frac{1+[n(1-\mathcal{R}_f)-1]\mathcal{R}_s e^{-2\alpha x}}{(1-\mathcal{R}_s)e^{-\alpha x}+\mathcal{T}(n-1)\mathcal{R}_s e^{-2\alpha x}}\,\mathcal{T}. \tag{A21}$$

Substituting Eq. (A21) into Eq. (A17), we finally obtain the exact solution for y_1:

$$y_1 = n\,\frac{(1-\mathcal{R}_f)(1-\mathcal{R}_s)e^{-\alpha x}-(1-\mathcal{R}_f\mathcal{R}_s e^{-2\alpha x})\mathcal{T}}{\{1+[n(1-\mathcal{R}_f)-1]\mathcal{R}_s e^{-2\alpha x}\}\mathcal{T}}. \tag{A22}$$

From Eq. (A3) and using the results of $\mathcal{T}_f$ and y_1 obtained above, the imaginary part is simply

$$y_2 = \sqrt{\frac{4n}{\mathcal{T}_f}-(y_1+n+1)^2}. \tag{A23}$$

5. Properties of the substrate

To find the frequency dependence of n and α, one needs to measure the total transmittance $\mathcal{T}_{\rm sub}(\omega)$ and reflectance $\mathcal{R}_{\rm sub}(\omega)$ of a bare substrate. The quantities can be deduced from Eq. (A14) by letting $d=0$ (thus $y=0$):

$$\mathcal{T}_{\rm sub} = \frac{(1-\mathcal{R}_s)^2 e^{-\alpha x}}{1-\mathcal{R}_s^2 e^{-2\alpha x}}, \tag{A24}$$

$$\mathcal{R}_{\rm sub} = \frac{1+(1-2\mathcal{R}_s)e^{2-\alpha x}}{1-\mathcal{R}_s^2 e^{-2\alpha x}}\,\mathcal{R}_s = (\mathcal{T}_{\rm sub}e^{-\alpha x}+1)\mathcal{R}_s. \tag{A25}$$

The algebra is simplified by solving first for $\mathcal{R}_s$ and $e^{-\alpha x}$. (It is straightforward to get n and κ once $\mathcal{R}_s$ and α are known.)

Note that all quantities are positive but less than unity, so that the conditions $0 \leqslant \{\mathcal{T}_{\rm sub}, \mathcal{R}_{\rm sub}, \mathcal{R}_s$, and $e^{-\alpha x}\} \leqslant 1$ hold. On substitution of $e^{-\alpha x} = (\mathcal{R}_{\rm sub}-\mathcal{R}_s)/\mathcal{T}_{\rm sub}\mathcal{R}_s$ obtained from Eq. (A25) into Eq. (A24), one finds

$$\mathcal{T}_{\rm sub} = \frac{(1-\mathcal{R}_s)^2(\mathcal{R}_{\rm sub}-\mathcal{R}_s)/\mathcal{T}_{\rm sub}\mathcal{R}_s}{1-(\mathcal{R}_{\rm sub}-\mathcal{R}_s)^2/\mathcal{T}_{\rm sub}^2}. \tag{A26}$$

It turns out that the cubic term of $\mathcal{R}_s$ in Eq. (A26) vanishes, and one can get a simple quadratic equation with a solution:

$$\mathcal{R}_s = \frac{-B \pm \sqrt{B^2-4AC}}{2A}, \tag{A27}$$

where $A = 2-\mathcal{R}_{\rm sub}$, $B = -(\mathcal{T}_{\rm sub}^2 - \mathcal{R}_{\rm sub}^2 + 2\mathcal{R}_{\rm sub}+1)$, and $C = \mathcal{R}_{\rm sub}$. The upper (+) sign in Eq. (A27) should be abandoned since one would otherwise have $\mathcal{R}_s > \mathcal{R}_{\rm sub}$ which violates Eq. (A25). Once $\mathcal{R}_s$ is found, the other unknown, $e^{-\alpha x}$, can be found simply using Eq. (A25); the absorption coefficient is $\alpha = -(\ln e^{-\alpha x})/x$.

*Present address: M/A-COM Inc., Microelectronics Division, 100 Chelmsford Street, Lowell, MA 01851.

†Present address: Brookhaven National Laboratory, Upton, NY 11973.

‡Present address: Fritz-Haber-Institut, Dept. of Surface Physics, Faradayweg 4-6, 14195 Berlin, Germany.

§Present address: Los Alamos National Laboratory, Los Alamos, NM 87545.

[1] J. Bardeen, L. N. Cooper, and J. R. Schrieffer, Phys. Rev. **108**, 1175 (1957).

[2] H. D. Drew and A. J. Sievers, Phys. Rev. Lett. **19**, 697 (1967).

[3] L. H. Palmer and M. Tinkham, Phys. Rev. **165**, 588 (1968).

[4] M. Tinkham, *Introduction to Superconductivity* (McGraw-Hill, New York, 1975 and Krieger, New York, 1980).

[5] L. C. Hebel and C. P. Slichter, Phys. Rev. **107**, 901 (1957).

[6] M. C. Nuss, P. M. Mankiewich, M. L. O'Malley, E. H. Westerwick, and P. B. Littlewood, Phys. Rev. Lett. **66**, 3305 (1991).

[7] D. A. Bonn, P. Dosanjh, R. Liang, and W. N. Hardy, Phys. Rev. Lett. **68**, 2390 (1992).

[8] F. Gao, J. W. Kruse, C. E. Platt, M. Feng, and M. V. Klein, Appl. Phys. Lett. **63**, 2274 (1993).

[9] K. Holczer, L. Forro, L. Mihaly, and G. Gruner Phys. Rev. Lett. **67**, 152 (1991).

[10] D. B. Romero, C. D. Porter, D. B. Tanner, L. Forro, D. Mandrus, L. Mihaly, G. L. Carr, and G. P. Williams, Phys. Rev. Lett. **68**, 1590 (1992).

[11] R. E. Walstedt, W. W. Warren, R. F. Bell, G. F. Brennert, G. P. Espinosa, R. J. Cava, L. F. Schneemeyer, and J. V. Waszczak, Phys. Rev. B **38**, 9299 (1988).

[12] P. C. Hammel, M. Takigawa, R. H. Heffner, Z. Fisk, and K. C. Ott, Phys. Rev. Lett. **63**, 1992 (1989).

[13] S. E. Barrett, D. J. Durand, C. H. Pennington, C. P. Slichter, T. A. Friedmann, J. P. Rice, and D. M. Ginsberg, Phys. Rev. B **41**, 6283 (1990).

[14] For a review of NMR data, see C. H. Pennington and C. P. Slichter, in *Physical Properties of High Temperature Superconductors II*, edited by D. M. Ginsberg (World Scientific, Singapore, 1990), p. 269.

[15] F. Marsiglio, Phys. Rev. B **44**, 5373 (1991).

[16] R. Akis and J. P. Carbotte, Solid State Commun. **78**, 393 (1991).

[17] D. A. Bonn, R. Liang, T. M. Riseman, D. J. Baar, D. C. Morgan, K. Zhang, P. Dosanjh, T. L. Duty, A. MacFarlane, G. D. Morris,

J. H. Brewer, W. N. Hardy, C. Kallin, and A. J. Berlinsky, Phys. Rev. B **47**, 11 314 (1993).

[18] F. Gao, D. B. Romero, D. B. Tanner, J. Talvacchio, and M. G. Forrester, Phys. Rev. B **47**, 1036 (1993).

[19] J. M. Chwalek, C. Uher, J. F. Whitaker, G. A. Mourou, J. Agostinelli, and M. Lelental, Appl. Phys. Lett. **57**, 1696 (1990).

[20] S. G. Han, Z. V. Vardeny, K. S. Wong, O. G. Symko, and G. Koren, Phys. Rev. Lett. **65**, 2708 (1990).

[21] Y. Liu, J. F. Whitaker, and C. Uher, Appl. Phys. Lett. **63**, 979 (1993).

[22] R. T. Collins, Z. Schlesinger, F. Holtzberg, C. Feild, U. Welp, G. W. Crabtree, J. Z. Liu, and Y. Fang Phys. Rev. B **43**, 8701 (1991).

[23] D. Mandrus, L. Forro, D. Koller, C. Kendziora, and L. Mihaly, Phys. Rev. B **46**, 8632 (1992).

[24] D. C. Mattis and J. Bardeen, Phys. Rev. **111**, 412 (1958).

[25] L. Leplae, Phys. Rev. B **27**, 1911 (1983).

[26] J. Chang and D. J. Scalapino, Phys. Rev. B **40**, 4299 (1989).

[27] Note in a case-I process, such a peak will be absent in Eq. (2) because the divergence of the density of states is balanced by the vanishing of the case-I coherence factor at $E \sim \Delta$ as seen in Eq. (3).

[28] X. D. Wu, D. Dijkkamp, S. B. Ogale, A. Inam, E. W. Chase, P. F. Miceli, C. C. Chang, J. M. Tarascon, and T. Venkatesan, Appl. Phys. Lett. **51**, 861 (1987); X. D. Wu, A. Inam, M. S. Hegde, T. Venkatesan, C. C. Chang, E. W. Chase, B. Wilkens, and J. M. Tarascon, Phys. Rev. B **38**, 9307 (1988).

[29] F. Gao, G. L. Carr, C. D. Porter, D. B. Tanner, S. Etemad, T. Venkatesan, A. Inam, B. Dutta, X. D. Wu, G. P. Williams, and C. J. Hirschmugl Phys. Rev. B **43**, 10 383 (1991).

[30] G. P. Williams, Nucl. Instrum. Methods, Phys. Res. Sect. A **291**, 8 (1990).

[31] Frederick Wooten, *Optical Properties of Solids* (Academic, New York, 1972).

[32] K. Kamarás, S. L. Herr, C. D. Porter, N. Tache, D. B. Tanner, S. Etemad, T. Venkatesan, E. Chase, A. Inam, X. D. Wu, M. S. Hegde, and B. Dutta, Phys. Rev. Lett. **64**, 84 (1990).

[33] J. Orenstein, G. A. Thomas, A. J. Millis, S. L. Cooper, D. H. Rapkine, T. Timusk, L. F. Schneemeyer, and J. V. Waszczak, Phys. Rev. B **42**, 6342 (1990).

[34] For a review, see D. B. Tanner and T. Timusk, in *Physical Properties of High Temperature Superconductors III*, edited by D. M. Ginsberg (World Scientific, Singapore, 1992), p. 363.

[35] D. A. Bonn, A. H. O'Reilly, J. E. Greedan, C. V. Stager, T. Timusk, K. Kamarás, and D. B. Tanner, Phys. Rev. B. **37**, 1574 (1988).

[36] S. L. Cooper, G. A. Thomas, J. Orenstein, D. H. Rapkine, M. Capizzi, T. Timusk, A. J. Millis, L. F. Schneemeyer, and J. V. Waszczak, Phys. Rev. B **40**, 11 358 (1989).

[37] G. A. Thomas, J. Orenstein, D. H. Rapkine, M. Capizzi, A. J. Millis, R. N. Bhatt, L. F. Schneemeyer, and J. V. Waszczak, Phys. Rev. Lett. **61**, 1313 (1988).

[38] T. Timusk, S. L. Herr, K. Kamarás, C. D. Porter, D. B. Tanner, D. A. Bonn, J. D. Garrett, C. V. Stager, J. E. Greedan, and M. Reedyk, Phys. Rev. B **38**, 6683 (1988).

[39] D. N. Basov, R. Liang, D. A. Bonn, W. N. Hardy, B. Dabrowski, M. Quijada, D. B. Tanner, J. P. Rice, D. M. Ginsberg, and T. Timusk, Phys. Rev. Lett. **74**, 598 (1995).

[40] P. J. Hirschfeld, W. O. Putikka, and D. Scalapino, Phys. Rev. Lett. **71**, 3705 (1993).

[41] D. J. Scalapino, Phys. Rep. **250**, 329 (1995).

[42] P. W. Anderson, Science **235**, 1196 (1987); in *Frontiers and Borderlines in Many Particle Physics*, edited by J. R. Schrieffer and R. A. Broglia (North-Holland, Amsterdam, 1989); Phys. Rev. Lett. **64**, 1839 (1990); Science **256**, 1526 (1992).

[43] R. E. Glover and M. Tinkham, Phys. Rev. **108**, 243 (1957); M. Tinkham, in *Far-infrared Properties of Solids*, edited by S. S. Mitra and S. Nudelman (Plenum, New York, 1970), p. 233.